ChemComm

COMMUNICATION

View Article Online
View Journal | View Issue

Cite this: *Chem. Commun.*, 2022, **58**, 11410

Received 9th July 2022,
Accepted 15th September 2022

DOI: 10.1039/d2cc03126d

rsc.li/chemcomm

Self-assembly of an MRI responsive agent under physiological conditions provides an extended time window for *in vivo* imaging†

Nishanth D. Tirukoti,[a] Liat Avram,[b] Reut Mashiach,[a] Hyla Allouche-Arnon[a] and Amnon Bar-Shir *[a]

An MRI-responsive agent that spontaneously self-assembles to a large supramolecular structure under physiological conditions was designed. The obtained assembly provides an extended time window for *in vivo* studies, as demonstrated for a fluorine-19 probe constructed to sense Zn^{2+} with ^{19}F-iCEST MRI, in the future.

Small molecular MRI responsive agents, also known as smart contrast agents,[1,2] are rationally designed to sense an analyte (*i.e.*, metal ion, metabolite, *etc.*), condition (*i.e.*, redox, pH, *etc.*), or enzymatic activity through a change in the obtained MRI signal. Among these agents, those designed to map metal ions were extensively developed in the last two decades,[3] and although designed for a range of ions,[4] those agents aimed to sense Zn^{2+} [5] and Ca^{2+},[6,7] have shown promising results.[8] For some applications, their fast response was not compromised by their fast clearance and allowed the spatial monitoring of Zn^{2+} secretion from functioning pancreatic tissues[9] or glucose-stimulated Zn^{2+} excretion from non-tumoral prostate.[10] Nevertheless, the fast washout rates of some MRI-responsive agents required continuous infusion throughout the study period to map ion-mediated brain activity[6] or brain pathology.[7] In addition, fluorine-19-based Zn^{2+}-responsive agents developed for *in vivo* mapping of the metal ion in the brain[11] and in an animal model of prostate cancer,[12] using the ^{19}F-iCEST approach,[13] required relatively long acquisition times, and thus, continuous infusion of the synthetic probe. To overcome the limitation of fast washout of the delivered MRI-responsive agent, alternatives are needed.

One strategy to prevent the use of injectable probes is to develop and implement genetically encoded biosensors for MRI detection of metal ions.[14] Another alternative to prevent the rapidly washed out small molecular probes is the use of large-sized MRI responsive agents. This includes ion responsive agents of a type of dendrimers[15] or iron-oxide nanoparticles[16,17] that could be detected for a long time at the region of interest after their injection, even when delivered at sub-microliter quantities. Inspired by the demonstrations that water-soluble benzene-1,3,5-tricarboxamides (BTAs) conjugates self-assemble under elevated temperatures to obtain supramolecular polymers,[18] we show here a novel strategy for very slow washout of relatively small MRI probes. Specifically, we developed a ^{19}F-MRI-responsive agent for Zn^{2+} that spontaneously self-assembled to large structures only upon its delivery to the tissue of interest, enabling the detection of a robust ^{19}F-MRI signal from the imaging agent, even 20 hours after its delivery.

We have started by synthesizing a potential ^{19}F-iCEST probe for Zn^{2+} MRI, as responsive agents of this type required prolonged infusion in order to allow robust ^{19}F-MRI of the delivered agent.[11,12] As a putative Zn^{2+} recognition moiety of the designed assembly, compound **1** was first synthesized with a PEG-10 as a linker for further conjugations to a BTA backbone, through a reductive amination (Fig. 1). ^{19}F-NMR studies of **1** in the presence of Zn^{2+} showed characteristic ^{19}F-NMR peaks of free and Zn^{2+}-bound **1** with a $\Delta\omega$ (related to the free **1**, set to 0 ppm) of +5 ppm, and indeed, a pronounced ^{19}F-iCEST effect of 25% was observed for a buffered solution containing 3 mM **1** and 60 μM Zn^{2+} at 37 °C (Fig. S1, ESI†). Then, **1** was reacted with benzene-1,3,5-tricarbonyl trichloride to form the tripod molecule **2** (Fig. 1). **2** has the BTA backbone conjugated to three hydrophilic moieties, and thus, the potential to form large supramolecular assemblies based on π–π interactions and hydrogen bonding[18–20] between adjacent molecules (Fig. S2, ESI†).

The ability of tripod **2** to form nano-sized supramolecular assemblies in aqueous solution was then studied and compared to the one-unit probe **1** at both 25 °C and 37 °C (Fig. 2). To this end, dynamic light scattering (DLS) measurements were

[a] *Department of Molecular Chemistry and Materials Science, Weizmann Institute of Science, Rehovot 7610001, Israel. E-mail: amnon.barshir@weizmann.ac.il*
[b] *Department of Chemical Research Support, Weizmann Institute of Science, Rehovot 7610001, Israel*

† Electronic supplementary information (ESI) available: Experimental details and supplementary figures. See DOI: https://doi.org/10.1039/d2cc03126d

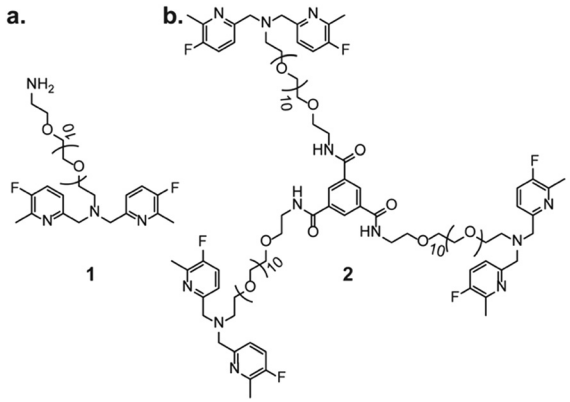

Fig. 1 The molecular structures of (a) **1** and (b) **2**.

first performed on aqueous solutions of **1** or **2** at either 25 °C or 37 °C. As expected, **1** showed a comparable size (D_h = 8.1 ± 1.6 nm and D_h = 9.2 ± 1.9 nm, at 25 °C and 37 °C, respectively) and a transparent solution at both studied temperatures (Fig. 2a), implying no formation of large assemblies even at an elevated temperature. Interestingly, a different observation was found for **2** when DLS measurements were performed at 25 °C (D_H = 54 ± 20.2 nm) or 37 °C (D_H = 163.3 ± 38.2 nm), indicating the formation of large assemblies when the solution of **2** was heated to a physiological temperature, 37 °C (Fig. 2c). Such large sizes obtained at 37 °C could also be detected by the naked eye, as shown from the pictures of tubes containing **2** at the two studied temperatures with white-colored assemblies appearing at 37 °C (Fig. 2c). Importantly, these assemblies are not just large-size precipitates, as they spontaneously disassembled when the solution was cooled to 25 °C to obtain their initial size and a clear solution (Fig. S3, ESI†).

To further elaborate on this observation, ^{19}F-NMR experiments were then performed on aqueous solutions of **1** or **2** at 25 °C and 37 °C. As depicted in Fig. 2b, for the solution of **1**, the same single peak was obtained in the ^{19}F-NMR spectrum at both studied temperatures. In contrast, for tripod **2**, a different observation could be detected at 25 °C and 37 °C. (Fig. 2d). While a single ^{19}F-NMR peak was observed at 25 °C, an additional peak, resonating 0.7 ppm upfield, was obtained when the sample was heated to 37 °C. Such an observation can be explained by the formation of a new chemical environment of the ^{19}F-entities of **2** upon temperature elevation and the assembly formation. To further explore this difference between the ^{19}F-NMR of **1** and **2**, and for a better understanding of the additional peak observed for **2** upon heating the solution to 37 °C, diffusion NMR experiments were performed as such studies are frequently used to determine the formation of large assemblies and differentiate them from the adjacent monomers in solution.[21] For **1**, a larger diffusion coefficient (D) of 0.48 ± 0.01 × 10^{-5} cm^2 s^{-1} was obtained at 37 °C, compared to that obtained at 25 °C, *i.e.*, 0.38 ± 0.01 × 10^{-5} cm^2 s^{-1} (Fig. 2b). This observation is expected for freely diffusing molecules that experience a faster Brownian motion at an elevated temperature and do not assemble to obtain larger structures. Interestingly, for tripod **2**, two different observations were obtained from the diffusion NMR experiments. While the ^{19}F-NMR peak that resonated at −128 ppm represents a monomeric diffusing moiety, which shows an increased diffusion coefficient upon

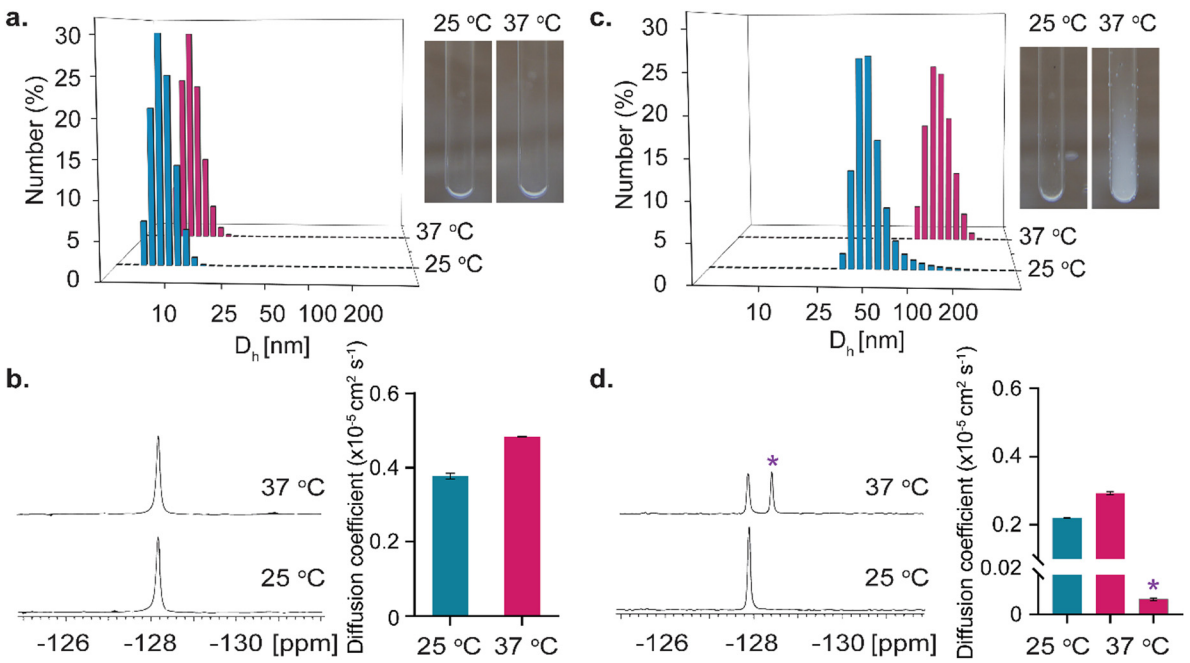

Fig. 2 Nano-assembly formation characterization. (a) DLS histograms of 100 μM **1** in water, with photographs of tubes containing 3 mM **1** at 25 °C and 37 °C. (b) ^{19}F-NMR spectra and ^{19}F-NMR diffusion coefficient plot of 3 mM **1** at 25 °C and 37 °C. (c) DLS plot of 100 μM **2** in water, with photographs of tubes containing 3 mM **2** at 25 °C and 37 °C. (d) ^{19}F-NMR spectra and ^{19}F-NMR diffusion coefficient plot of 3 mM **2** at 25 °C and 37 °C. in (d), * represents the peak of the nano-assembly of **2** obtained only at 37 °C.

heating the sample from 25 °C ($D = 0.22 \pm 0.01 \times 10^{-5}$ cm^2 s^{-1}) to 37 °C ($D = 0.29 \pm 0.01 \times 10^{-5}$ cm^2 s^{-1}), the additional peak appeared at 37 °C (0.7 ppm upfield) reflected a diffusion characteristic of a much larger structure (Fig. 2d). Significantly, the diffusion ^{19}F-NMR experiments of **2** revealed that this peak (marked with * in Fig. 2d) represented a molecular structure that had a very low diffusion coefficient ($D = 0.008 \pm 0.001 \times 10^{-5}$ cm^2 s^{-1}). This slow diffusion rate, 38 times slower compared to that obtained at 37 °C for the molecular entity represented by the peak at −128 ppm (Fig. 2d), strengthened our conclusion that a large assembly of **2** is obtained at 37 °C. Importantly, the ability of **2** to self-assemble to large entities was not affected by pH values that are expected in biological systems (Fig. S4 and S5, ESI†).

Then, to examine the feasibility of **2** for use in future studies to sense Zn^{2+}, its ability to bind the metal ion was studied with ^{19}F-NMR. To this end, an aqueous solution containing 2 mM of **2** (*i.e.*, 6 mM of chelating units) and 1.2 mM of Zn^{2+} (5 : 1 chelate : Zn^{2+} ratio) was examined and an additional peak was obtained with a large and specific chemical shift offset relative to the resonance of free ligand **2** ($\Delta\omega$ = +5 ppm, Fig. S6, ESI†). Note that at higher Zn^{2+} concentrations, beyond those expected in biological systems, the peak of **2**-Zn^{2+} complex is clearly observed in the ^{19}F-NMR spectrum but the peak that is assigned with the large assembly is reduced (Fig. S8, ESI†). Importantly, at such high Zn^{2+} levels even the presence of higher concentrations of Cu^{2+} (2 times more than Zn^{2+}), the ^{19}F-NMR peak of **2**-Zn^{2+} complex was still preserved (Fig. S9, ESI†). Then, as one of the main advantages of ^{19}F-iCEST is to amplify signals of low levels of ions, the Zn^{2+} concentration was further diluted to obtain a solution with 2 mM **2** and 80 μM of Zn^{2+} and ^{19}F-iCEST experiments were performed (Fig. 3a). Here, where the Zn^{2+} ion was 75 times more diluted than the chelating units (3 units per one tripod **2**), a pronounced 27% ^{19}F-iCEST effect was obtained. Such an effect that was obtained with the sensitivity of 12 mM of ^{19}F-nuclei (150 times more concentrated than Zn^{2+} set at 80 μM) corresponded to a 40 times signal amplification effect in the ^{19}F-MRI framework. This ^{19}F-iCEST effect obtained for **2** and Zn^{2+}, although milder than that obtained with a more flexible ^{19}F-chelate,[11] was much larger than that obtained with a ^{19}F-chelates based on the BAPTA backbone.[12]

Having confirmed the formation of nano-sized assemblies of **2** at a physiological temperature of 37 °C (Fig. 2) and its Zn^{2+} binding capability (Fig. 3), we examined whether our designed supramolecular probe could be used as a Zn^{2+}-specific ^{19}F-iCEST MRI agent when compared to other cations. For that purpose, a phantom composed of seven different test tubes containing 80 μM of biologically relevant cations (*e.g.*, K^+, Mg^{2+}, Cu^{2+}, Zn^{2+}, Ca^{2+}, Na^+, or no ion) in the presence of 2 mM **2** was prepared, and MRI was performed on a 9.4 T MRI scanner at 37 °C. Note here that the addition of these cations at the expected biological levels did not affect the assembly process of **2** (Fig. S10 and S11, ESI†). As depicted in Fig. 3b, ^{1}H-MRI showed no signal difference between the examined tubes, confirming that the assembly of **2** did not give rise to contrast changes. A similar observation was made for ^{19}F-MRI where

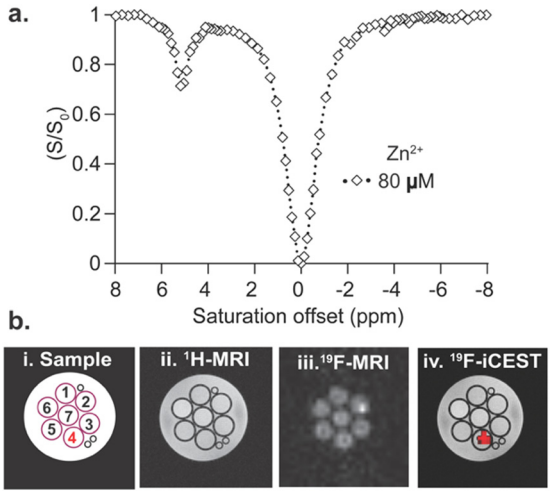

Fig. 3 ^{19}F-iCEST of **2**. (a) ^{19}F-iCEST spectrum (*i.e.*, z-spectrum) obtained from the aqueous solution of 2 mM **2** in the presence of 80 μM of Zn^{2+}. (b) ^{19}F-iCEST MRI: (i) schematic representation of the studied phantom composed of seven tubes containing 2 mM **2** and 80 μM cation (pH-7.4), *i.e.*, (1) Mg^{2+}, (2) Cu^{2+}, (3) Na^+, (4) Zn^{2+}, (5) K^+, (6) Ca^{2+} and (7) no ion; (ii) ^{1}H-MRI; (iii) ^{19}F-MRI; (iv) ^{19}F-iCEST map obtained at $\Delta\omega$ = +5 ppm. Experiments were performed at 37 °C on 9.4 T NMR (a) or 9.4 T MRI (b).

identical ^{19}F-signal was detected for all 7 examined tubes. Nevertheless, a ^{19}F-iCEST MRI experiment that was performed on the very same phantom resulted in a clear signal reduction at $\Delta\omega$ = +5 ppm, only from the Zn^{2+} containing tube. Overlaying the ^{19}F-iCEST contrast on the ^{1}H-MR image represented the spatial distribution of the cation and presented as a Zn^{2+}-map (Fig. 3b, z-spectrum shown in Fig. S12, ESI†).

Finally, after confirming the stability of the large-assembly of **2** in biological media for 24 hours (Fig. S13, ESI†), we aimed to examine whether the transition of **2** to a large assembly under physiological condition would affect its washout profile *in vivo*. For that purpose, 1 μL of either **1** or tripod **2** (dissolved in DMSO, which did not affect the assembly and ^{19}F-iCEST appearance of **2**, Fig. S14, ESI†) at an equal fluorine-19 concentration was intracranially injected into the hippocampus of the mouse brain. The examined mice were placed in a 15.2 T MRI scanner and longitudinal ^{19}F-MR studies were performed (Fig. 4). As expected from low-molecular-weight imaging agents, such as **1** (Fig. 2a and b), the ^{19}F-NMR signal could be detected only 30 min after the intracranial injection of the solution of **1**, with much of the probe washed out as fast as one hour after the injection (Fig. 4a). This fast washout does not allow for sufficient time to perform ^{19}F-MRI experiments (Fig. S15, ESI†) and requires the use of continued infusions of the agent, as previously shown for small probes.[11,12] In contrast, the ^{19}F-NMR signal of the injected probe **2** was preserved for more than 20 hours after its delivery (Fig. 4b), although injected at the same concentration as **1**. ^{19}F-MRI experiments performed 30 min and 21 hours after its delivery showed the localization of **2** at the injection site even one day after its injection, confirming its very slow washout (Fig. 4c) without significant damage of the tissue (Fig. S17 and S18, ESI†). These results confirm that

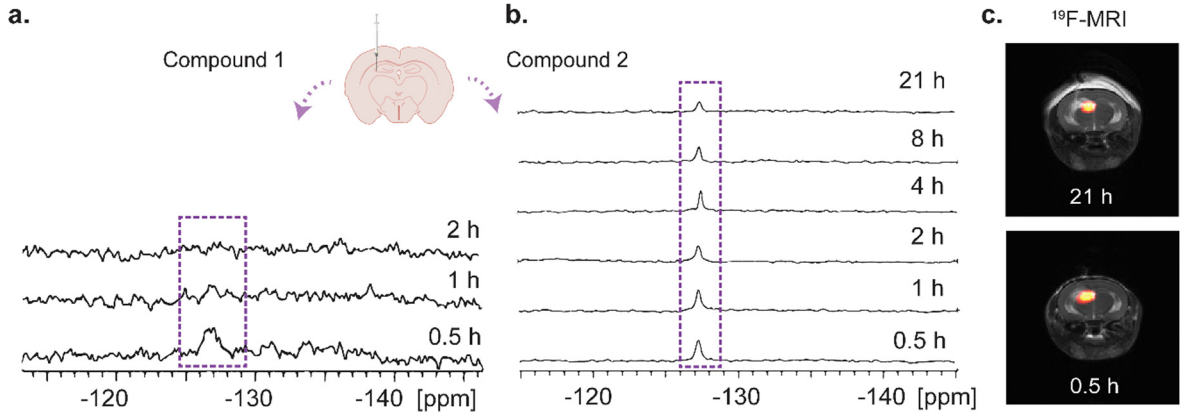

Fig. 4 *In vivo* ^{19}F-NMR and ^{19}F-MRI. (a) ^{19}F-NMR spectra of a live mouse obtained 0.5 h, 1 h, 2 h after intracranial injection of **1** (1 μL of 225 mM in DMSO, 0.1 μL min^{-1} rate). (b) ^{19}F-NMR spectra of a live mouse obtained 0.5 h, 1 h, 2 h, 4 h, 8 h, 21 h after intracranial injection of **2** (1 μL of 75 mM in DMSO, 0.1 μL min^{-1} rate). (c) ^{19}F-MRI of the same animal for which the NMR spectrum is shown in (b) at 0.5 h and 21 h after delivery of **2**.

the spontaneous assembly of **2** to a large moiety upon its delivery, prevented its clearance from the injected site.

To summarize, we showed here a conceptually novel approach to slow down the washout rate of imaging agents from their region of delivery through their spontaneous self-assembly. By conjugating a ^{19}F-iCEST probe (**1**) to an aromatic BTA motif to obtain a tripod type molecular architecture (**2**), the tendency of the obtained structure to form nano-assemblies at 37 °C was demonstrated. *In vivo* experiments of an injected **2** revealed a prolonged ^{19}F-MRI signal without the need for continuous infusion strategies used currently in MRI studies of low-molecular-weight responsive probes.[6,7,11,12] Adopting the principles used in this study, a similar molecular design can be applied to a wide range of imaging sensors that require prolonged imaging times or for those that cannot tolerate fast washout rates.

This work was supported by the Israel Science Foundation (ISF 1329/20) and the Minerva Foundation.

Conflicts of interest

There are no conflicts to declare.

Notes and references

1 G. Angelovski and E. Toth, *Chem. Soc. Rev.*, 2017, **46**, 324–336.
2 J. Wahsner, E. M. Gale, A. Rodriguez-Rodriguez and P. Caravan, *Chem. Rev.*, 2019, **119**, 957–1057.
3 W.-h Li, S. E. Fraser and T. J. Meade, *J. Am. Chem. Soc.*, 1999, **121**, 1413–1414.
4 E. L. Que and C. J. Chang, *Chem. Soc. Rev.*, 2010, **39**, 51–60.
5 A. J. Lubag, L. M. De Leon-Rodriguez, S. C. Burgess and A. D. Sherry, *Proc. Natl. Acad. Sci. U. S. A.*, 2011, **108**, 18400–18405.
6 A. Barandov, B. B. Bartelle, C. G. Williamson, E. S. Loucks, S. J. Lippard and A. Jasanoff, *Nat. Commun.*, 2019, **10**, 897.
7 T. Savic, G. Gambino, V. S. Bokharaie, H. R. Noori, N. K. Logothetis and G. Angelovski, *Proc. Natl. Acad. Sci. U. S. A.*, 2019, **116**, 20666–20671.
8 V. Clavijo Jordan, C. D. G. Hines, L. T. Gantert, S. Wang, S. Conarello, C. Preihs, S. Chirayil, M. Klimas, J. L. Evelhoch and A. D. Sherry, *Front. Endocrinol.*, 2021, **12**, 641722.
9 A. F. Martins, V. Clavijo Jordan, F. Bochner, S. Chirayil, N. Paranawithana, S. Zhang, S. T. Lo, X. Wen, P. Zhao, M. Neeman and A. D. Sherry, *J. Am. Chem. Soc.*, 2018, **140**, 17456–17464.
10 M. V. Clavijo Jordan, S. T. Lo, S. Chen, C. Preihs, S. Chirayil, S. Zhang, P. Kapur, W. H. Li, L. M. De Leon-Rodriguez, A. J. Lubag, N. M. Rofsky and A. D. Sherry, *Proc. Natl. Acad. Sci. U. S. A.*, 2016, **113**, E5464–E5471.
11 N. D. Tirukoti, L. Avram, T. Haris, B. Lerner, Y. Diskin-Posner, H. Allouche-Arnon and A. Bar-Shir, *J. Am. Chem. Soc.*, 2021, **143**, 11751–11758.
12 Y. Yuan, Z. Wei, C. Chu, J. Zhang, X. Song, P. Walczak and J. W. M. Bulte, *Angew. Chem., Int. Ed.*, 2019, **58**, 15512–15517.
13 A. Bar-Shir, A. A. Gilad, K. W. Chan, G. Liu, P. C. van Zijl, J. W. Bulte and M. T. McMahon, *J. Am. Chem. Soc.*, 2013, **135**, 12164–12167.
14 H. F. Ozbakir, A. D. C. Miller, K. B. Fishman, A. F. Martins, T. E. Kippin and A. Mukherjee, *ACS Sens.*, 2021, **6**, 3163–3169.
15 S. Gunduz, N. Nitta, S. Vibhute, S. Shibata, M. E. Mayer, N. K. Logothetis, I. Aoki and G. Angelovski, *Chem. Commun.*, 2015, **51**, 2782–2785.
16 A. Bar-Shir, L. Avram, S. Yariv-Shoushan, D. Anaby, S. Cohen, N. Segev-Amzaleg, D. Frenkel, O. Sadan, D. Offen and Y. Cohen, *NMR Biomed.*, 2014, **27**, 774–783.
17 S. Okada, B. B. Bartelle, N. Li, V. Breton-Provencher, J. J. Lee, E. Rodriguez, J. Melican, M. Sur and A. Jasanoff, *Nat. Nanotechnol.*, 2018, **13**, 473–477.
18 N. M. Matsumoto, R. P. M. Lafleur, X. Lou, K. C. Shih, S. P. W. Wijnands, C. Guibert, J. van Rosendaal, I. K. Voets, A. R. A. Palmans, Y. Lin and E. W. Meijer, *J. Am. Chem. Soc.*, 2018, **140**, 13308–13316.
19 X. Lou, R. P. M. Lafleur, C. M. A. Leenders, S. M. C. Schoenmakers, N. M. Matsumoto, M. B. Baker, J. L. J. van Dongen, A. R. A. Palmans and E. W. Meijer, *Nat. Commun.*, 2017, **8**, 15420.
20 R. P. M. Lafleur, S. M. C. Schoenmakers, P. Madhikar, D. Bochicchio, B. Baumeier, A. R. A. Palmans, G. M. Pavan and E. W. Meijer, *Macromolecules*, 2019, **52**, 3049–3055.
21 L. Avram and Y. Cohen, *Chem. Soc. Rev.*, 2015, **44**, 586–602.